Hindawi
Advances in Civil Engineering
Volume 2020, Article ID 6241789, 9 pages
https://doi.org/10.1155/2020/6241789

Research Article

Experiment Study on Dynamic Effects of Tower-Line Systems Induced by Ice Shedding

Xianzhong Xie,[1,2] **Yuanjie Wu**,[1] **Kaiyuan Liang**,[1] **Sai Liu**,[1] **and Jian Peng**[1,2]

[1]*School of Civil Engineering, Hunan University of Science and Technology, Xiangtan 411201, Hunan, China*
[2]*Hunan Provincial Key Laboratory of Structures for Wind Resistance and Vibration Control, Hunan University of Science and Technology, Xiangtan 411201, China*

Correspondence should be addressed to Xianzhong Xie; xianzhongx@163.com

Received 3 December 2019; Accepted 21 January 2020; Published 26 February 2020

Academic Editor: Khalid Abdel-Rahman

Taking the 220 kV transmission line as the prototype, a test model of the double-span tower-line system with a scale ratio of 1 : 20 was proposed on the basis of dynamic similarity theory. 14 different working conditions including zippered, simultaneous, entire, and local ice-shedding were controlled and realized by use of the program-controlled mode. The displacement transient responses of transmission line under these ice-shedding conditions were analyzed in detail. The results show that the variation laws of the ice-shedding dynamic-load coefficient and the jump height with the velocity, quantity, and position of the ice-shedding are obtained, which can provide references for the design of the transmission tower-line system.

1. Introduction

Because of the long-term exposure in the field, the transmission tower-line system is inevitably affected by various external factors. Under the action of temperature, wind power, mechanical external force, etc., ice-shedding jump will be produced by the ice-covered transmission conductor. The violent oscillation of the conductor will cause interphase flashovers and the destruction of fittings or other components, the occurrence of line fracture, and tower collapse. At present, the research on the ice-shedding jump of the transmission conductor mainly focuses on theoretical analyses, field measurement, test model, and numerical simulation; meanwhile, the last two methods are dominant. Furthermore, the previous research studies on numerical simulation are relatively comprehensive and careful, and this paper mainly focuses on the test model.

At present, the galloping phenomenon is one of the important sources of electrical/mechanical failures in transmission lines (see [1]). The ice covering of the conductor is one of the necessary factors in causing galloping (see [2]). As the transmission line is a large-span flexible structure, it has properties similar to the cable. So, in the study of the dynamics of transmission lines, we use the relevant dynamics theory of the cable for reference (see [3–8]). In theory, Rega and Lacarbonara performed many studies on the nonlinear free and forced vibrations of the transmission lines (see [9, 10]). The vibration of a single conductor transmission line with a Stockbridge damper was studied by using the double-beam theory (see [11, 12]). Based on the Lagrange equation, Peng deduced the analytical dynamics equation of transmission line ice shedding theoretically. And the quantitative analysis was carried out (see [13]). According to energy conservation, stress-sag relation, geometrical relation of spans, and equilibrium of suspension insulators of multispan transmission lines after ice shedding, Wu et al. proposed the theoretical method for calculating the maximum jump of transmission lines (see [14]). Xie et al. studied the dynamic characteristics of two-span suspended transmission lines and introduced the frequency avoidance phenomenon (see [15]). In terms of numerical simulation, Kálmán et al. established the dynamic model of ice shedding of a single-span overhead transmission conductor and obtained the failure criterion of glazed ice incorporating both axial and bending effects (see [16]). Kollar et al. conducted numerical analysis on the improved model and revealed the relationship between the distance of the thickness of the ice coating and adjacent spacers and the

displacement, tension, and jump height generated by the transmission conductor (see [17]). Mirshafiei et al. obtained the accurate simulation of the propagation effect of cross fracture of overhead transmission line, which is necessary to predict the cross-ice dynamic response of transmission line after fracture (see [18]). Yan et al. simulated the galloping of the ice transmission line and obtained the galloping characteristics of the iced transmission lines with and without internal resonance in steady and stochastic wind fields (see [19]). Ji et al. conducted a quantitative analysis of the mechanical deicing method for shock load overhead transmission lines (see [20]). In the test model, Morgan and Swift conducted a test on a 132 kV five-span transmission line and obtained the jump height of the release of simulated ice loads from the central span, which showed that sag was an important factor in the jump height (see [21]). Jamaleddine et al. designed a reduced-scale model of two-span overhead transmission line, and the span length is only 3.22 m. By model tests, the maximum jump height and tension change of each hanging point of the overhead line were obtained (see [22, 23]). Xia conducted a simulated experiment of ice shedding in isolated span and measured the tension at the middle of the line (see [24]). Kollár et al. conducted the wet-snow-shedding experiment of a single overhead line in the freezing laboratory to simulate the shedding process of wet snow under various natural conditions (see [25]). Meng et al. made a simulation study of ice shedding in isolated span and continuous span and measured the jump height of the conductor (see [26]). Yang et al. used a single conductor to simulate the ice-shedding phenomenon between isolated span and found that the max dynamic tension caused by part of ice shedding from the conductor may be larger than the whole ice shedding (see [27]). Lu et al. studied the aerodynamic parameters of crescent-shaped and D-shaped conductors by the wind tunnel test and obtained that wind velocity, ice thickness, conductor type, bundle spacing, and splitting number all have a great influence on aerodynamic parameters and conductor galloping (see [28]).

The abovementioned literature studies focus on ice-shedding theory, numerical simulation, and model experiments, but the experiments are not comprehensive enough. This paper aims to use test models and comprehensively considers the model's dynamic similarity, the diversity of multispan coupling and ice-shedding conditions. Based on the specific engineering background, the experimental model was derived. And according to the requirement of the dynamic similarity, the parameters of the system were designed. Therefore, the model experiment presented in this paper can reflect the dynamic characteristics of the actual project. The three-tower and two-span continuous model can reflect the coupled vibration and rule between the span and the span during the ice-shedding process. In addition, a program-controlled method was used to control the shedding of the simulated ice load, so the various complicated ice-shedding conditions in the project can be simulated effectively.

The paper is organized as follows: In Section 2, the relevant design of the experimental model and the experimental conditions are given. In Section 3, the experimental correlation analysis and results are illustrated. Finally, the conclusions are presented in Section 4.

2. Experimental Design

2.1. Background of the Project. The test model is based on a 220 kV transmission line project. The crossing form of the conductor is that the two tensile towers are at the ends, and the tangent tower is in the middle. The first span is 352 m, and the second is 248 m. At both ends of the model are tensile towers with a structural height of 34 m and a base heel of 9.21 m. The middle part is a tangent tower with a structural height of 55 m and a base heel of 8.68 m. The wire uses the LGJ-400/30 steel core aluminum strand wire. The suspension insulator string type is TZ-2, and the tensile insulator string type is SDN-323.

2.2. Transmission Line Design. In the test, the transmission conductor uses steel wires instead. The elastic modulus (E_m) of the conductor is 209 GPa, and the comprehensive elastic modulus (E_p) of the prototype conductor is 69 GPa, so the similarity ratio of the elastic modulus of the transmission conductor is

$$C_E = \frac{E_m}{E_p} = 3.03. \tag{1}$$

Due to the limitations of the laboratory, the maximum value of geometric similarity ratio is about

$$C_l = \frac{1}{20}. \tag{2}$$

According to the dynamic similarity criterion, other model parameters are shown in Table 1.

Based on the dynamic similarity criterion, the line density of the conductor model is up to 229 g/m, while the line density of the steel wire used in the experiment is only 8.8 g/m. This problem can be resolved by counterweight. The counterweight of the conductor model is 220.2 g/m by use of the lead rod.

2.3. Equivalent Tower Design. This paper mainly studies the ice-shedding dynamic characteristics of transmission conductors. As the stiffness of the tower is much greater than the one of the transmission line, the tower has less impact on the transmission line. Therefore, the design of the transmission tower model adopts an equivalent design strategy so that the global dynamic characteristic is similar. The members of the equivalent tower are made of round steel pipes. Taking the frequency similarity ratio of the previous-two-order as the objective function, the parameter values of the equivalent tower can be obtained by optimization algorithm. The transmission line is hinged to the tension tower by a tension insulator, and the mass and length of the insulator are also designed on the basis of dynamic similarity theory.

2.4. Test System and Test Conditions. The experimental model of the tower-line system is shown in Figure 1, and the test system of the ice-shedding test is shown in Figure 2. The first span is 17.6 m, which is the deicing span. The transmission conductor and the tension tower are connected by

Table 1: Similarity ratio and values of model parameters.

Model parameters	Similar relationship	Similarity ratio	Parameter value
Outer diameter (m)	$C_l = l_m/l_p$	1/20	1.38×10^{-3}
Elastic modulus (MPa)	$C_E = E_m/E_p$	3.03	2.09×10^{-5}
Linear density (kg·m^{-1})	$C_\rho = C_E/C_l$	3.03/20	0.229
Design stress (MPa)	$C_\sigma = C_E/C_\varepsilon$	3.03	181.8
First span length (m)	$C_l = l_m/l_p$	1/20	17.6
Second span length (m)	$C_l = l_m/l_p$	1/20	12.4
Time (s)	$C_t = C_l^{1/2}$	1/4.472	—
Frequency (Hz)	$C_f = C_l^{-1/2}$	4.472	—
Velocity (m·s^{-1})	$C_v = C_l^{1/2}$	1/4.472	—

Figure 1: The experimental model of tower-line system.

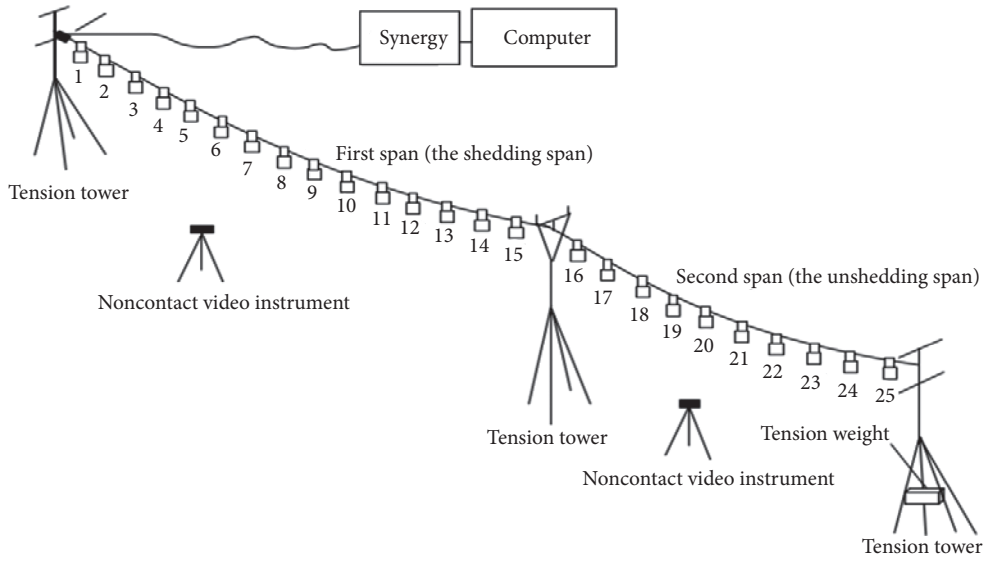

Figure 2: Schematic diagram of the test system.

the tension sensor. The second span is 12.4 m, which is the un-deicing span. The tension and the line profile were adjusted by controlling the mass of the tension weight by placing the tension weight near the end of the tension tower. The deicing span arranged 15 mass units named as 1 to 15 by uniform distribution along the conductor. The non-deicing span arranged 10 mass units named as 16 to 25 by uniform distribution along the conductor. The displacement response of the transmission conductor during the process was tested by a noncontact video instrument.

Table 2: Comparison of test sags and theoretical sags.

Displacement test point	Test sag (m)	Theoretical sag (m)	Error (%)
First-span point 4	0.321	0.324	0.93
First-span point 8	0.430	0.432	0.46
First-span point 12	0.322	0.324	0.62
Second-span midpoint	0.210	0.214	1.87

Table 3: Comparison of test frequency and design frequency.

Research object	Vibration mode	Test frequency (Hz)	Design frequency (Hz)	Error (%)
Tension tower	First order	23.05	22.15	4.07
	Second order	23.49	22.46	4.56
Tangent tower	First order	7.625	7.813	2.47
	Second order	7.678	7.861	2.38
First-span conductor	First order	0.804	0.830	3.23
	Second order	1.058	1.074	1.51
Second-span conductor	First order	1.131	1.172	3.62
	Second order	1.631	1.709	4.78

2.5. Shape of Line and Modal Verification. In order to ensure the correctness of line alignment of the tower-line system under the action of self-weight and counterweight, the sags of four test points of the two spans were measured by laser rangefinder. After the comparison between the experimental sags and the theoretical sags, the result shows that maximum error is less than 1.87% (see Table 2).

After the spectrum analysis of the acceleration signal of the free vibration of tower and line, we can obtain that the experimental model modes and the test frequency are consistent with the design frequency. The maximum error is less than 4.78% (see Table 3).

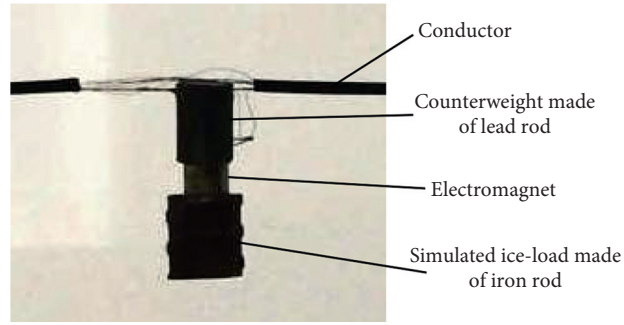

Figure 3: Simulated ice load and control device of ice shedding.

2.6. Ice-Shedding Conditions. Figure 3 shows simulated ice loading and shedding control devices. The simulation of ice shedding is realized by the action of electromagnet on iron. By controlling the power switch of electromagnet programmatically, various ice-shedding conditions of the conductor can be simulated. Table 4 shows simulated ice-shedding conditions, where $\lambda = 1/4.472$ is the velocity similarity ratio.

3. Experimental Results and Discussion

3.1. Ice-Shedding Transient Response. According to the above 14 working conditions in sequence, the ice-shedding tests are carried out to obtain the displacement-time response data of the measuring points under all kinds of working conditions. Figure 4 shows the displacement-time history curve of the midpoint of the ice-shedding span under different ice-shedding velocities (I ~ VI). The dynamic response of the transmission conductor will increase with the ice-shedding velocity. At the low ice-shedding velocity, the dynamic response of the transmission conductor is similar to the static unloading process. The greater the ice-shedding velocity, the more similar the dynamic response of the transmission conductor to the simultaneous ice-shedding process.

Figure 5 shows the displacement-time history curve of the midpoint of ice-shedding span under different ice-shedding quantities (VI ~ IX). The dynamic response of the transmission conductor will increase with ice-shedding quantity. But their vibration trend is basically consistent.

Figure 6 shows the displacement-time history curve of the midpoint of ice-shedding positions under different ice-shedding positions (X ~ XIV). When local ice shedding occurs in the middle of the span, the dynamic response of the transmission conductor is the largest. With the ice-shedding position approaching the towers, the dynamic response gradually decreases. But the response contains more frequency components.

3.2. Jump Height and Dynamic-Load Coefficient. The jump height is defined as

$$H_j = H_m - H_i, \tag{3}$$

where H_m denotes the maximum height that the midpoint of transmission line or ice-shedding area can reach after ice-shedding and H_i denotes the initial height of the midpoint of transmission line or ice-shedding area in the static equilibrium position. On the basis of H_j, the dynamic-load coefficient is defined as

Table 4: Ice-shedding conditions of the model.

Conditions	Serial number	Ice-shedding form	Ice-shedding position	Ice-shedding velocity (m/s)	Ice-shedding quantity (%)	Measuring point position
Different ice-shedding velocities	I	Zipper-like ice shedding	1–15	10λ	100	Point 8 (middle of span)
	II	Zipper-like ice shedding	1–15	25λ	100	
	III	Zipper-like ice shedding	1–15	50λ	100	
	IV	Zipper-like ice shedding	1–15	75λ	100	
	V	Zipper-like ice shedding	1–15	100λ	100	
Different ice-shedding quantities	VI	Simultaneous ice shedding	1–15	—	100	Point 8 (middle of span)
	VII	Simultaneous ice shedding	7–9	—	20	
	VIII	Simultaneous ice shedding	6–10	—	33	
	IX	Simultaneous ice shedding	5–11	—	47	
Different ice-shedding locations	X	Simultaneous ice shedding	1–3	—	20	Point 2
	XI	Simultaneous ice shedding	4–6	—	20	Point 5
	XII	Simultaneous ice shedding	7–9	—	20	Point 8 (middle of span)
	XIII	Simultaneous ice shedding	10–12	—	20	Point 11
	XIV	Simultaneous ice shedding	13–15	—	20	Point 14

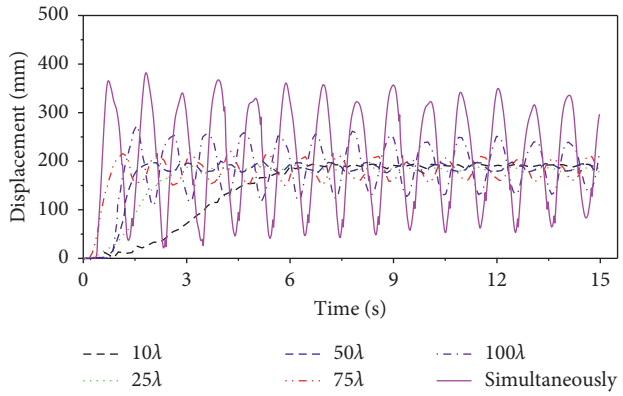

Figure 4: Displacement-time history curve of the midpoint of ice-shedding span under different ice-shedding velocities (I ~ VI).

$$\eta_{dl} = \frac{H_j}{H_s}, \tag{4}$$

where H_s denotes the static displacement of the midpoint of transmission line or ice-shedding area, which is caused by static load of slow ice shedding.

Figure 7 illustrates the relationship between the jump height of the midpoint of the ice-shedding span and the ice-shedding velocity. With the increase of the ice-shedding velocity, the jump height curves show a rising trend and finally tend to the jump height (382 mm) under the simultaneous ice shedding.

Figure 8 shows the relation curve of the dynamic-load coefficient of the midpoint of the ice-shedding span and the ice-shedding velocity. The value of dynamic-load coefficient shows a rising trend with the increase of the ice-shedding velocity and finally tends to 2.1, which is close to the theoretical value of dynamic-load coefficient of the sudden load. Hence, it is reasonable to simplify the simultaneous ice shedding of the whole span to a sudden load.

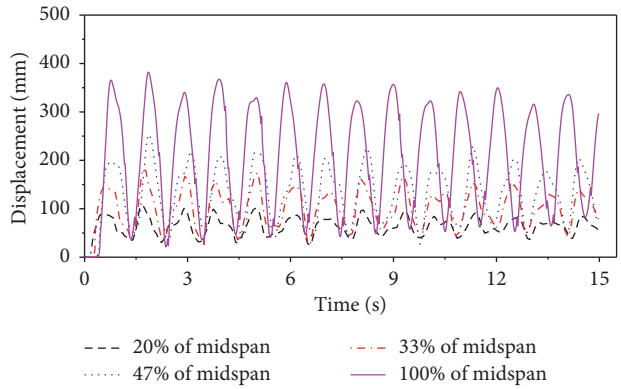

Figure 5: Displacement-time history curve of the midpoint of ice-shedding span under different ice-shedding quantities (VI ~ IX).

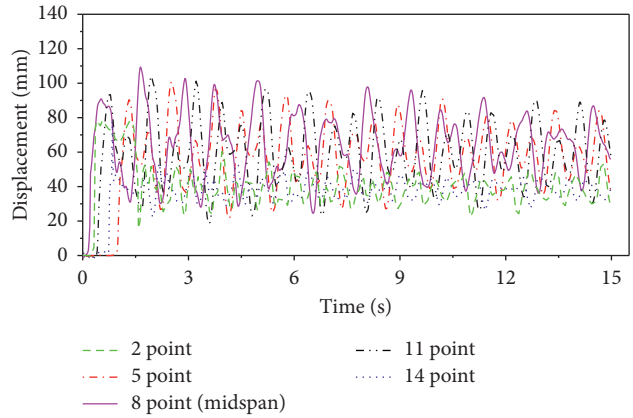

Figure 6: Displacement-time history curve of the midpoint of ice-shedding area under different ice-shedding positions (X ~ XIV).

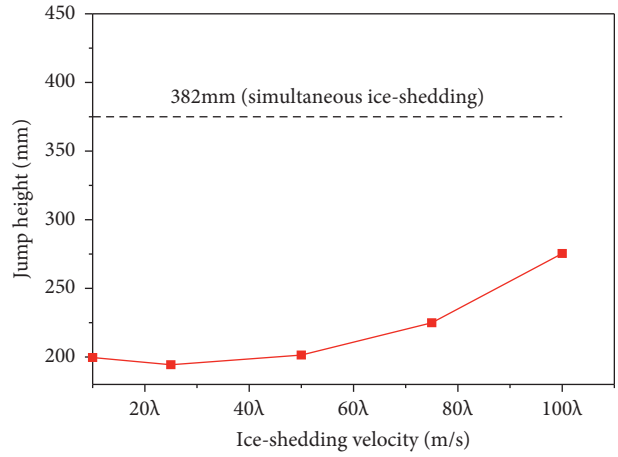

Figure 7: The variation of the jump height with ice-shedding velocity.

Figure 9 shows the relation curve of the jump height of the midpoint of the ice-shedding span and the ice-shedding quantity. As ice-shedding quantity increases, the jump height which occurs during 60 mm–390 mm generally increases linearly.

Figure 10 shows the relationship between dynamic-load coefficient of the midpoint of the ice-shedding span and ice-shedding quantity. From 20% to 100% ice-shedding quantity, the dynamic-load coefficient, which is about 1 to 2.1, approximately increases linearly.

Figure 11 shows that the change of the midpoint of ice-shedding area has influence on the jump height. From point 2 to point 14, the jump height, which is about 75 mm to 110 mm, first increases and then decreases with a similar

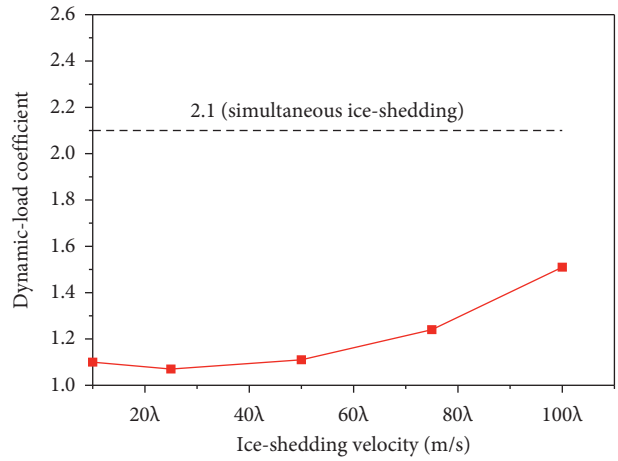

Figure 8: The variation of the dynamic-load coefficient with ice-shedding velocity.

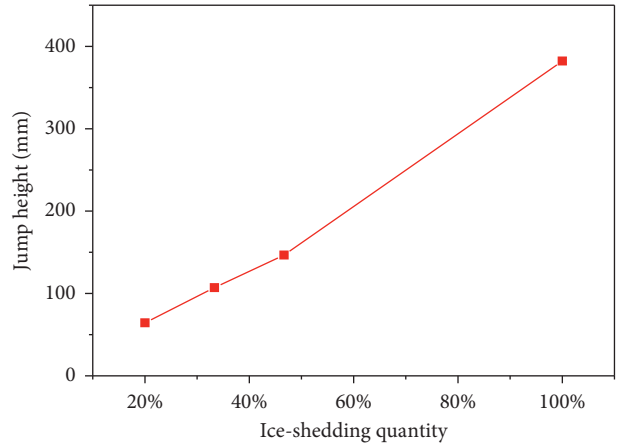

Figure 9: The variation of the jump height with ice-shedding quantity.

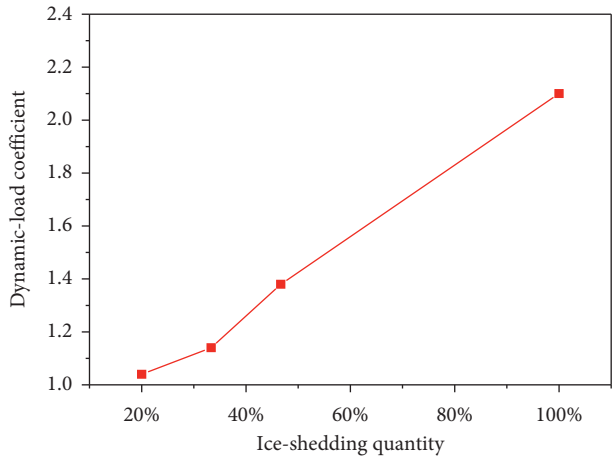

Figure 10: The variation of the dynamic-load coefficient with ice-shedding quantity.

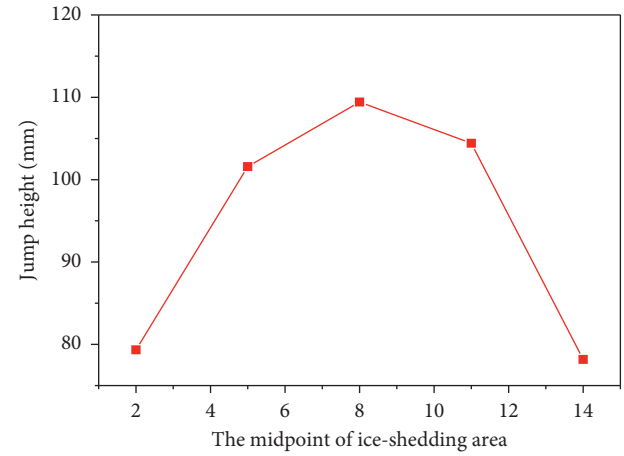

Figure 11: The variation of the jump height with the midpoint of ice-shedding area.

trend, and the peak value occurs at point 8. If partial ice shedding occurs at the midspan, the jump height has the largest value. With the ice-shedding area approaching the towers, the jump height will gradually decrease.

Figure 12 shows the relationship between the dynamic-load coefficient and the ice-shedding position. If partial ice shedding occurs at the midspan, the dynamic-load coefficient comes to the minimum value. With the ice-shedding area

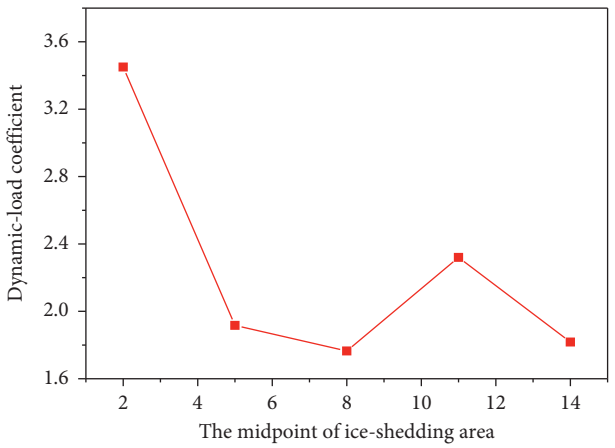

Figure 12: The variation of the dynamic-load coefficient with the midpoint of ice-shedding area.

approaching the towers, the dynamic-load coefficient will gradually increase. The dynamic-load coefficients of the symmetric point 2 and point 14 have great difference, which is mainly due to the fact that the point 2 is close to the tension tower so that the constraint stiffness is larger, while point 14 is close to the straight tower, where exists the coupling effect between the spans so that the constraint stiffness is smaller.

4. Conclusions

In this paper, the dynamic response of the tower-line system is analyzed by the test model under various working conditions, such as ice-shedding velocities, ice-shedding quantities, and ice-shedding positions. Then, the conclusions are as follows:

The peak value of the displacement response of the transmission line will increase with the increase of ice-shedding velocity. The smaller the ice-shedding velocity, the more similar the ice-shedding response to the static unloading. The larger the ice-shedding velocity, the more similar the ice-shedding response to the simultaneous ice-shedding. The jump height and the dynamic-load coefficient tend to increase with the increase of ice-shedding velocity. The dynamic-load coefficient of the simultaneous ice-shedding is close to the theoretical value of the dynamic-load coefficient of the sudden load.

Under different conditions of ice-shedding quantity, the dynamic response of the transmission line is basically synchronized and the amplitude will increase with the increase of ice-shedding quantity. The jump height and the dynamic-load coefficient are basically proportional to the ice-shedding quantity.

When partial ice-shedding occurs at the midspan, the dynamic-load coefficient is relatively small, while the jump height value is relatively large. With the ice-shedding area approaching the towers, the jump height will gradually decrease and the dynamic-load coefficient will tend to increase.

In terms of the jump height of the conductor, the simultaneous ice-shedding is the most dangerous working condition and the maximum jumping height of the transmission line can reach 2% of the length of the ice-shedding span [21].

Data Availability

All data included in this study are available upon request by contact with the corresponding author.

Conflicts of Interest

The authors declare that they have no conflicts of interest.

Acknowledgments

This study was supported by the National Natural Science Foundation of China (Grant no. 11272119) and Scientific Research Fund of Hunan Provincial Education Department (Grant no. 19B192).

References

[1] N. A. Saadabad, H. Moradi, and G. Vossoughi, "Semi-active control of forced oscillations in power transmission lines via optimum tuneable vibration absorbers: with review on linear dynamic aspects," *International Journal of Mechanical Sciences*, vol. 87, pp. 163–178, 2014.

[2] L. Zhang, Q. Li, Z. lv, K. Ji, and B. Liu, "Research on the test of transmission line galloping," *IOP Conference Series: Earth and Environmental Science*, vol. 128, Article ID 012123, 2018.

[3] D. M. Brotton, "Cable structures, by h. max irvine, mit press, cambridge, mass., 1981. no. of pages: 259. price: £28·00," *Earthquake Engineering & Structural Dynamics*, vol. 10, no. 2, p. 347, 1982.

[4] A. H. Nayfeh, H. N. Arafat, C.-M. Chin, and W. Lacarbonara, "Multimode interactions in suspended cables," *Journal of Vibration and Control*, vol. 8, no. 3, pp. 337–387, 2002.

[5] G. Rega, "Nonlinear vibrations of suspended cables—part I: modeling and analysis," *Applied Mechanics Reviews*, vol. 57, no. 6, pp. 443–478, 2004.

[6] S. Lenci and L. Ruzziconi, "Nonlinear phenomena in the single-mode dynamics of a cable-supported beam," *International Journal of Bifurcation and Chaos*, vol. 19, no. 3, pp. 923–945, 2009.

[7] L. Wang and G. Rega, "Modelling and transient planar dynamics of suspended cables with moving mass," *International Journal of Solids and Structures*, vol. 47, no. 20, pp. 2733–2744, 2010.

[8] Y. Zhao, Z. Guo, C. Huang, L. Chen, and S. Li, "Analytical solutions for planar simultaneous resonances of suspended cables involving two external periodic excitations," *Acta Mechanica*, vol. 229, no. 11, pp. 4393–4411, 2018.

[9] G. Rega, "Theoretical and experimental nonlinear vibrations of sagged elastic cables," in *Nonlinear Dynamic Phenomena in Mechanics*, pp. 159–210, Springer, Dordrecht, Netherlands, 2012.

[10] W. Lacarbonara, *Nonlinear Structural Mechanics: Theory, Dynamical Phenomena and Modeling*, Springer Science & Business Media, Berlin, Germany, 2013.

[11] O. Barry, J. W. Zu, and D. C. D. Oguamanam, "Forced vibration of overhead transmission line: analytical and

experimental investigation," *Journal of Vibration and Acoustics*, vol. 136, no. 4, Article ID 041012, 2014.

[12] O. Barry, J. Zu, and D. Oguamanam, "Analytical and experimental investigation of overhead transmission line vibration," *Journal of Vibration and Control*, vol. 21, no. 14, pp. 2825–2837, 2015.

[13] F. Peng, "Dynamic characteristics of overhead transmission lines following ice shedding based on Lagrange equation," in *Proceedings of the International Power, Electronics & Materials Engineering Conference*, Atlantis Press, Dalian, China, May 2015.

[14] C. Wu, B. Yan, L. Zhang, B. Zhang, and Q. Li, "A method to calculate jump height of iced transmission lines after ice-shedding," *Cold Regions Science and Technology*, vol. 125, pp. 40–47, 2016.

[15] X. Xie, X. Hu, J. Peng, and Z. Wang, "Refined modeling and free vibration of two-span suspended transmission lines," *Acta Mechanica*, vol. 228, no. 2, pp. 673–681, 2017.

[16] T. Kálmán, M. Farzaneh, and G. Mcclure, "Numerical analysis of the dynamic effects of shock-load-induced ice shedding on overhead ground wires," *Computers & Structures*, vol. 85, no. 7-8, pp. 375–384, 2007.

[17] L. E. Kollar and M. Farzaneh, "Vibration of bundled conductors following ice shedding," *IEEE Transactions on Power Delivery*, vol. 23, no. 2, pp. 1097–1104, 2008.

[18] F. Mirshafiei, G. Mcclure, and M. Farzaneh, "Modelling the dynamic response of iced transmission lines subjected to cable rupture and ice shedding," *IEEE Transactions on Power Delivery*, vol. 28, no. 2, pp. 948–954, 2013.

[19] B. Yan, X. Liu, X. Lv, and L. Zhou, "Investigation into galloping characteristics of iced quad bundle conductors," *Journal of Vibration and Control*, vol. 22, no. 4, pp. 965–987, 2016.

[20] K. Ji, B. Liu, Y. Cheng, X. Zhan, and G. McClure, "Evaluation and optimization of a shock load de-icing method for transmission lines with combined ice failure criteria," *Cold Regions Science and Technology*, vol. 165, Article ID 102818, 2019.

[21] V. T. Morgan and D. A. Swift, "Jump height of overhead-line conductors after the sudden release of ice loads," *Proceedings of the Institution of Electrical Engineers*, vol. 111, no. 10, pp. 1736–1746, 1964.

[22] A. Jamaleddine, G. McClure, and J. Rousselet, "Physical and numerical simulations of ice-shedding effects on a reduced-scale model of overhead transmission line," in *Proceedings of the International Symposium on Cable Dynamics*, vol. 1, Liege, Belgium, October 1995.

[23] A. Jamaleddine, R. Beauchemin, J. Rousselet, and G. McClure, "Weight-dropping simulation of ice-shedding effects on an overhead transmission line model," in *Proceedings of the 7th International Workshop on Atmospheric Icing of Structures*, pp. 44–48, Chicoutimi, Canada, June 1996.

[24] Z. Xia, *Research on Galloping and Ice-Shedding of Ultra High-Voltage Transmission Conductors*, Ph.D. thesis, Huazhong University of Science & Technology, Wuhan, China, 2008.

[25] L. E. Kollár, O. Olqma, and M. Farzaneh, "Natural wet-snow shedding from overhead cables," *Cold Regions Science and Technology*, vol. 60, no. 1, pp. 40–50, 2010.

[26] X. Meng, L. Wang, L. Hou et al., "Dynamic characteristic of ice-shedding on UHV overhead transmission lines," *Cold Regions Science & Technology*, vol. 66, no. 1, pp. 44–52, 2011.

[27] W. G. Yang, S. B. Su, and Z. Q. Wang, "Experiment study on dynamic effects of ice shedding on overhead transmission line," *Advanced Materials Research*, vol. 710, pp. 306–310, 2013.

[28] J. Lu, Q. Wang, L. Wang et al., "Study on wind tunnel test and galloping of iced quad bundle conductor," *Cold Regions Science and Technology*, vol. 160, pp. 273–287, 2019.